Charge transport, specific heat, and optical properties across the metal-insulation transition in $Ba_{3-x}R_xNb_5O_{15}$

Wataru Sekino,[1] Ryosuke Takei,[1] Satomi Ito,[1] Haruki Takei,[1] Kenta Iwamoto,[1] Yumiko Katayama,[2] Kazunori Ueno,[2] Hideki Kuwahara,[3] and Takuro Katsufuji[1,4]

[1]*Department of Physics, Waseda University, Tokyo 169-8555, Japan*
[2]*Department of Basic Science, University of Tokyo, Meguro, Tokyo 153-8902, Japan*
[3]*Department of Physics, Sophia University, Tokyo 169-8555, Japan*
[4]*Kagami Memorial Research Institute for Materials Science and Technology, Waseda University, Tokyo 169-0051, Japan*

(Received 29 August 2023; revised 7 October 2023; accepted 7 November 2023; published 11 December 2023)

We studied barium niobates with a tetragonal tungsten bronze structure in which Ba is substituted by various rare earths including divalent Eu and trivalent La, Ce, Pr, Nd, and Sm. The magnitude of the negative magnetoresistance observed for $Ba_{3-x}Eu_xNb_5O_{15}$ increases near the metal-insulator phase boundary of a series of compounds at $x \sim 2.2$, where the number of carriers estimated using the Hall coefficient decreases by two orders of magnitude from that of the parent compound. Various transport properties, specific heat, and the optical reflectivity spectra of the series of compounds were measured and it was found that all the results can be explained by the changes in the number of carriers n and the effective mass m^*, except for the anomalous decrease in the Seebeck coefficient from $x = 0$ to 1.

DOI: 10.1103/PhysRevMaterials.7.124404

I. INTRODUCTION

Transition-metal oxides often exhibit various intriguing phenomena arising from a strong Coulomb interaction between the electrons of d orbitals in transition metals. One of the most fascinating phenomena is the presence of insulating states caused by the Coulomb interaction (Mott insulators) and a phase transition between a Mott-insulating state and a metallic state induced by variations in temperature, doping concentration, and applied pressure, called Mott transitions [1]. Mott transitions occur in various $3d$ transition-metal oxides, but some of the $4d$ and $5d$ transition-metal oxides, for example, pyrochlore $R_2Mo_2O_7$ [2–4] and $R_2Ir_2O_7$ [5–7], and $(Ca, Sr)_2RuO_4$ [8,9] also exhibit Mott transitions.

$Ba_3Nb_5O_{15}$ [10–17] has a tetragonal tungsten bronze structure [10,13] as illustrated in Fig. 1, where there are 0.2 nominal $4d$ electrons per Nb. This compound is metallic with one order of magnitude lower resistivity along the c axis [15] and exhibits superconductivity below ~1.5 K [13]. A series of compounds with the substitution of Ba by Sr, $Ba_{3-x}Sr_xNb_5O_{15}$, however, become insulating when $x > 2$, even though both Ba and Sr are divalent and, thus, the number of $4d$ electrons per Nb does not change with x. According to Ref. [15], the insulating state in $Ba_{3-x}Sr_xNb_5O_{15}$ is different from that in conventional Mott insulators. Recently, it has been found that a series of compounds with the substitution of Ba by divalent Eu, $Ba_{3-x}Eu_xNb_5O_{15}$, also exhibit a metal-insulator transition at $x \sim 2.2$. Furthermore, these compounds exhibit a large negative magnetoresistance, whose absolute value amounts to $\rho(0)/\rho(H) \sim 5 \times 10^3$, where $\rho(H)$ is the resistivity at the magnetic field H, near the metal-insulator phase boundary [16]. It is likely that the negative magnetoresistance arises from the coupling between the conduction electrons in the $4d$ orbital of Nb and the localized $4f$ spins of Eu, and the metal-insulator transition plays an important role in the increase in the magnitude of negative magnetoresistance.

In Ref. [16], $Ba_{3-x}R_xNb_5O_{15}$ with only $R =$ Eu was investigated but a series of compounds with the substitution of Ba by trivalent R have not been investigated. Furthermore, although the resistivity and magnetic susceptibility have been investigated, the origin of the metal-insulator transition in $Ba_{3-x}Eu_xNb_5O_{15}$, which may critically affect its large magnetoresistance, has not been clarified. In this study, we grew single crystals of $Ba_{3-x}R_xNb_5O_{15}$ [11] with $R =$ La, Ce, Pr, Nd, Sm, and Eu, and measured their various physical properties to clarify how the electronic structure changes with the substitution of Ba in $Ba_{3-x}R_xNb_5O_{15}$ and also why the negative magnetoresistance increases for $R =$ Eu at the metal-insulator phase boundary of $x \sim 2.2$.

II. EXPERIMENT

Single crystals of $Ba_{3-x}R_xNb_5O_{15}$ were grown by the floating-zone technique as described in Ref. [16]. Resistivity was measured by a conventional four-probe technique with a silver paste cured at room temperature as electrodes. Magnetoresistance was measured by applying a magnetic field at various directions, but significant dependence on the directions of the magnetic field was not observed and thus, the resistivity along the c axis with the applied magnetic field along the a axis is shown in this paper. Magnetic susceptibility was measured using a SQUID magnetometer. Hall resistivity was measured by applying a magnetic field between −7 and 7 T along the b axis while applying the electric current along

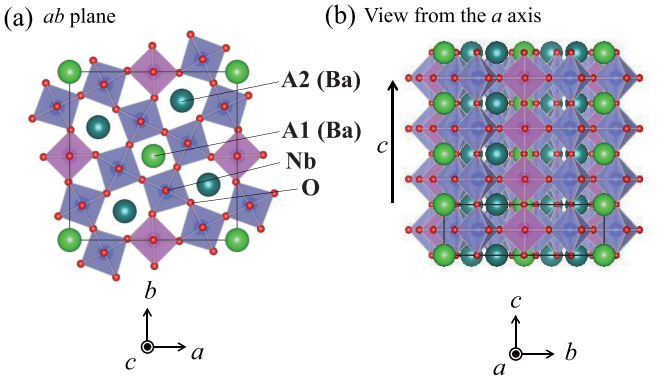

FIG. 1. Crystal structure of $Ba_3Nb_5O_{15}$ (a) along the *ab* plane and (b) seen from the *a* axis drawn by VESTA [18].

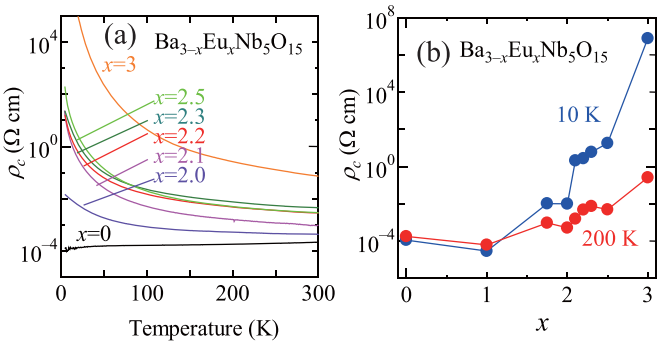

FIG. 3. (a) Temperature dependence of resistivity and (b) x dependence of resistivity at 10 and 200 K both along the c axis for $Ba_{3-x}Eu_xNb_5O_{15}$.

the c axis and measuring the voltage along the a axis. Since the effect of large negative magnetoresistance overlapped the Hall signal for R = Eu, the difference between the voltage at H and the voltage at $-H$ was taken to remove such effect. Thermopower was measured by a conventional steady-state method both along the c axis and the a axis. Specific heat was measured by a relaxation technique. Optical reflectivity was measured at room temperature on the polished ac plane of the single crystals using a grating spectrometer between 0.7 and 5 eV and an FTIR spectrometer between 0.1 and 0.8 eV.

III. RESULTS

Figure 2 shows the 420 peak in the x-ray powder diffraction of the grown single crystals for $Ba_{3-x}La_xNb_5O_{15}$. As can be seen, the peak is broad and seems to split into two peaks for $x = 0.5$. There are two inequivalent sites of Ba ions for $Ba_3Nb_5O_{15}$, A1 and A2 [10,13], as illustrated in Fig. 1. For $Ba_{3-x}La_xNb_5O_{15}$ with $x = 1$, all the A1 sites, which are tightly bound to surrounding oxygen ions, are occupied by La with a smaller ionic radius whereas all the A2 sites are occupied by Ba. Thus, it is likely that the composition of $x = 1$ is stable and the compounds with $0 < x < 1$ tend to be separated into phases with $x = 0$ and 1, resulting in the splitting of the x-ray diffraction peaks. Furthermore, we found that it is difficult to grow the crystals with $x > 1$ for $Ba_{3-x}R_xNb_5O_{15}$ with trivalent R. Therefore, we investigated only $Ba_2RNb_5O_{15}$ with

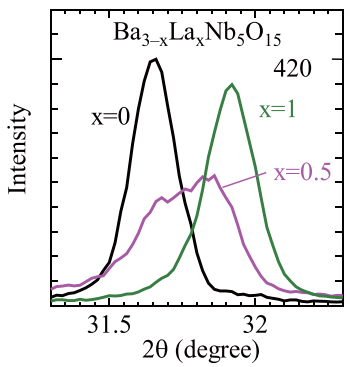

FIG. 2. The 420 peak in the x-ray diffraction pattern of $Ba_{3-x}La_xNb_5O_{15}$ with $x = 0$, 0.5, and 1.0.

trivalent R. For $Ba_{3-x}Eu_xNb_5O_{15}$, crystals can be grown over $0 \leqslant x \leqslant 3$ without any instability. This is probably because Eu is divalent and, thus, there is no change in the valence of Nb, and also because the ionic radius of divalent Eu is not as small as trivalent La and close to Ba. The x-ray powder diffraction patterns over a wider range of 2θ and the lattice constants are shown in the Appendix.

In Ref. [16], the T dependence and the magnetic field H dependence of the resistivity ρ for $Ba_{3-x}Eu_xNb_5O_{15}$ were measured over a wide range of x. As a continuation of the previous study, they were measured in more details near the metal-insulator phase boundary of $x \sim 2.2$. Figure 3(a) shows the resistivity as a function of T at various values of x and Fig. 3(b) shows the resistivity at 10 and 200 K as a function of x. A metal-insulator crossover around $x \sim 2.2$ is clearly observed.

$\rho(H)/\rho(0)$ is plotted as a function of H at various temperatures (T) for $x = 2.0$, 2.2, and 2.5 in Figs. 4(a)–4(c). As

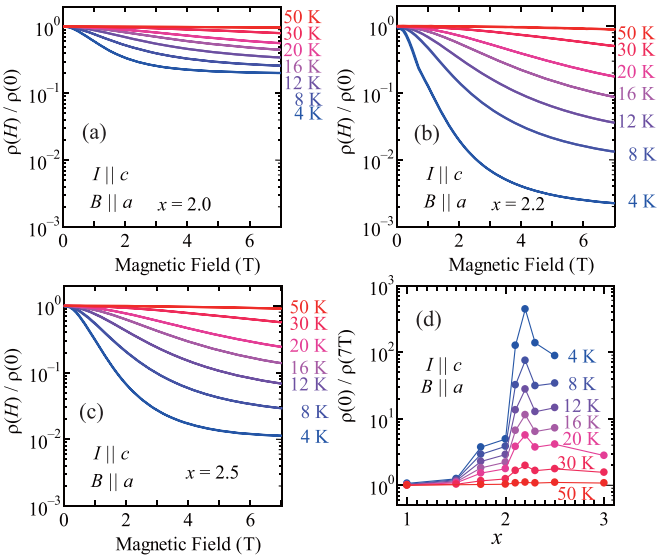

FIG. 4. (a)–(c) Resistivity ρ at H [$\rho(H)$] divided by that at $H = 0$ [$\rho(0)$] on a logarithm scale as a function of H for $Ba_{3-x}Eu_xNb_5O_{15}$ with (a) $x = 2.0$, (b) 2.2, and (c) 2.5. (d) Magnitude of magnetoresistance defined as $\rho(0)/\rho(7T)$ at various T values as a function of x for $Ba_{3-x}Eu_xNb_5O_{15}$.

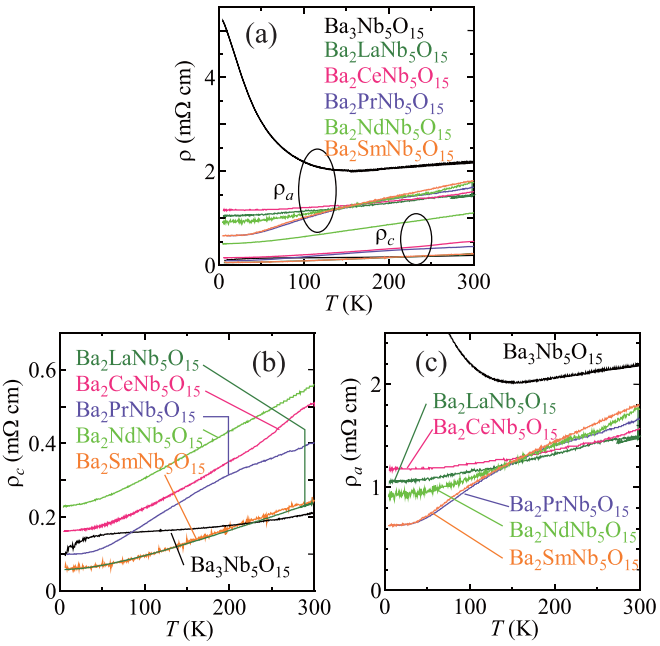

FIG. 5. (a), (b) Temperature dependence of resistivity for $Ba_2RNb_5O_{15}$ with various rare earths R (a) both along the c (ρ_c) and a (ρ_a) axes, (b) along the c axis (ρ_c) only, and (c) along the a axis (ρ_a) only.

can be seen, the resistivity decreases with increasing H, and it decreases more with decreasing T, and it decreases the most at $x = 2.2$. To examine the x dependence more clearly, the magnitude of the magnetoresistance defined as $\rho(0)/\rho(H)$ at $H = 7$ T is plotted as a function of x at various T values in Fig. 4(d). At all T values, $\rho(0)/\rho(H)$ is maximum at $x = 2.2$, indicating that the negative magnetoresistance increases near the metal-insulator phase boundary in $Ba_{3-x}Eu_xNb_5O_{15}$.

Figure 5 shows the T dependence of resistivity for $Ba_2RNb_5O_{15}$, together with that for the parent compound $Ba_3Nb_5O_{15}$. As can be seen, $d\rho/dT$ is positive for all the data, indicating a metallic character of $Ba_2RNb_5O_{15}$. Furthermore, the resistivity along the c axis, ρ_c, is lower than that along the a axis, ρ_a, for all the compounds, similarly to the behavior of the parent compound. For the parent compound, $d\rho_a/dT$ is positive for $T > 150$ K, but ρ_a shows an upturn at $T \sim 150$ K and $d\rho_a/dT$ becomes negative for $T < 150$ K, although $d\rho_c/dT$ is positive over the entire T range [15]. Note that ρ_c does not diverge at the lowest T but remains finite, indicating that the ground state is a highly anisotropic conventional metallic state. However, such an anomaly in $\rho_a(T)$ disappears for the R-doped compounds, and both $d\rho_c/dT$ and $d\rho_a/dT$ are positive over the entire T range.

The magnetic susceptibility of $Ba_2RNb_5O_{15}$ along the c (χ_c) and a (χ_a) axes is plotted on a logarithm scale as a function of T in Fig. 6. Depending on the species of R, the magnitude of magnetic susceptibility at 300 K changes from less than 1×10^{-4} mol/cm^3 for $R =$ La without $4f$ moments to $\sim 5 \times 10^{-3}$ mol/cm^3 for $R =$ Nd and Pr with $4f$ moments. Figure 7 shows the inverse magnetic susceptibility $1/\chi$ of $Ba_2RNb_5O_{15}$ with $R =$ Ce, Pr, Nd, and Sm. $1/\chi$ follows an almost straight line, a Curie-Weiss behavior, and

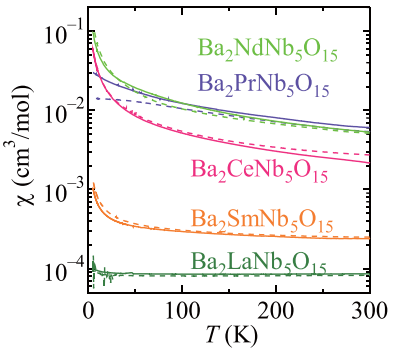

FIG. 6. Temperature dependence of magnetic susceptibility on a logarithm scale for $Ba_2RNb_5O_{15}$ with various rare earths R along the c (solid lines) and a (dashed lines) axes.

the Curie constant c obtained by the fitting of χ_c and χ_a to $\chi = C/(T + \theta)$ is consistent with the theoretical values of the magnetic moment for trivalent Ce, Pr, Nd, and Sm ions, as shown in the Appendix. This indicates that Ce, Pr, Nd, and Sm are all trivalent in $Ba_2RNb_5O_{15}$. Nevertheless, one can see that χ_c and χ_a are slightly different from each other and that the T dependence of $1/\chi$ is slightly away from a straight line. Such characteristics in $1/\chi$ are different from those for $Ba_{3-x}Eu_xNb_5O_{15}$ [16], suggesting the role of the multiplets of the $4f$ states in the magnetic susceptibility for trivalent $R =$ Ce, Pr, Nd, and Sm.

To determine the number of carriers in $Ba_{3-x}R_xNb_5O_{15}$, Hall measurement was conducted. H dependence of the Hall resistivity is shown in the Appendix. Figure 8(a) shows the Hall coefficient along the ac plane R_{ac} estimated from the Hall resistivity for the parent compound and $Ba_2RNb_5O_{15}$ with $R =$ La or Pr. As can be seen, R_{ac} is always negative, indicating that the carriers are electrons, and the absolute value

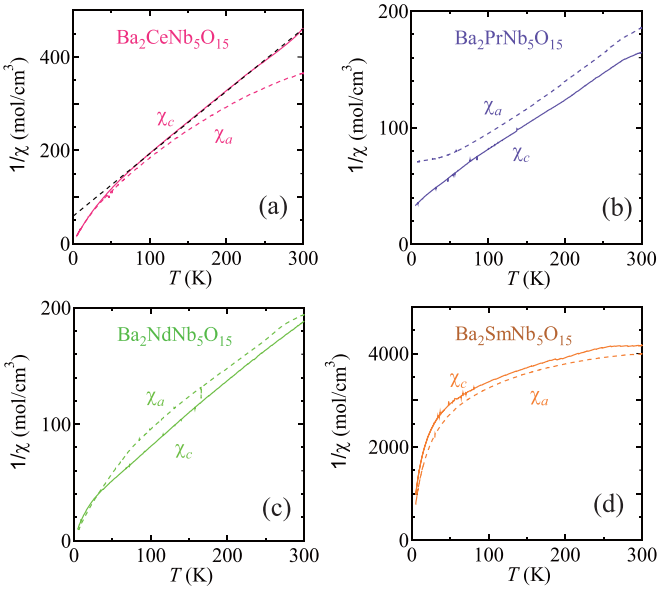

FIG. 7. Inverse magnetic susceptibility as a function of T for $Ba_2RNb_5O_{15}$ along the c (solid lines) and a (dashed lines) axes for (a) $R =$ Ce, (b) Pr, (c) Nd, and (d) Sm.

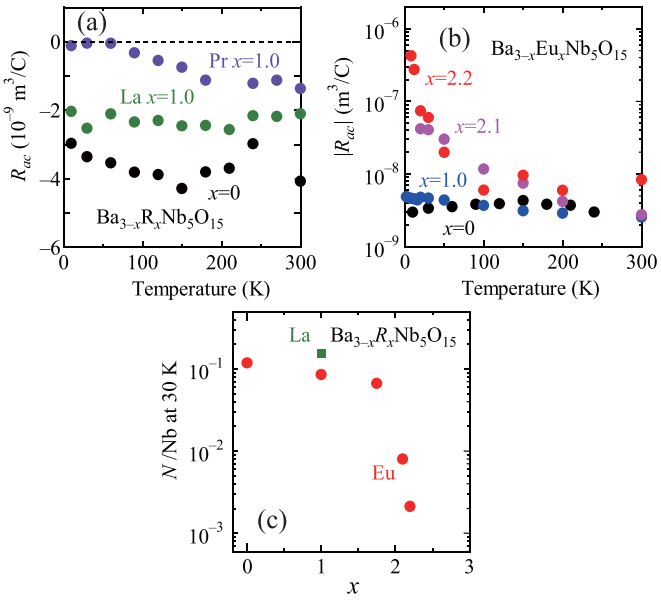

FIG. 8. (a) Hall coefficient along the *ac* plane, where the voltage along the *b* axis was measured while the current density is along the *c* axis and the magnetic field is along the *a* axis, as a function of T for $Ba_3Nb_5O_{15}$ and $Ba_2RNb_5O_{15}$ with R = La and Pr. (b) Absolute values of the Hall coefficient along the *ac* plane as a function of T for $Ba_{3-x}Eu_xNb_5O_{15}$ with $x = 0$, 1.0, 2.1, and 2.2. (c) The number of carriers per Nb estimated from the Hall coefficient at 30 K as a function of x for $Ba_{3-x}R_xNb_5O_{15}$ with R = Eu (circles) and La (a square).

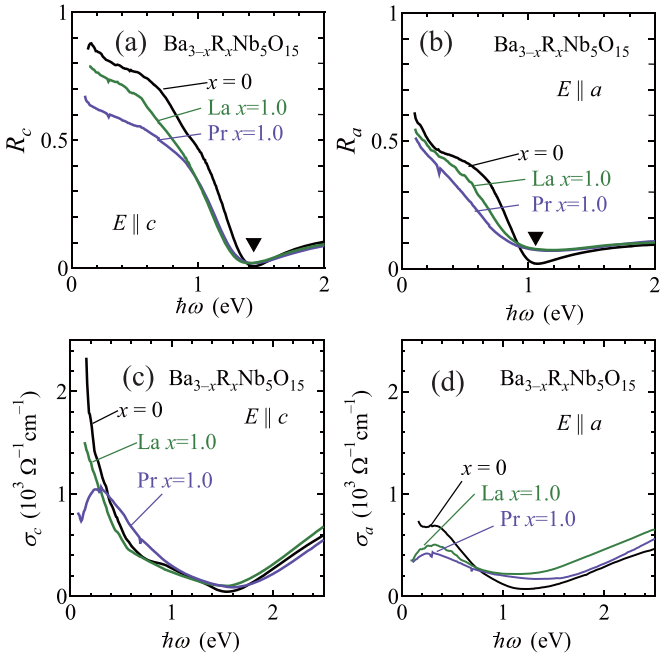

FIG. 9. (a), (b) Reflectivity and (c), (d) optical conductivity spectra with the polarization along the (a), (c) *c* and (b), (d) *a* axes for $Ba_3Nb_5O_{15}$ and $Ba_2RNb_5O_{15}$ with R = La and Pr.

of R_{ac} is 4×10^{-9} m^3/C, corresponding to ∼0.1 electrons per Nb, for the parent compound [15], but it decreases to 2×10^{-9} m^3/C or less for $Ba_2RNb_5O_{15}$ with R = La or Pr. This result is qualitatively consistent with the increase in the nominal number of d electrons per Nb from 0.2 to 0.4 with the substitution of R^{3+} for Ba^{3+}.

On the other hand, the sign of R_{ac} for $Ba_{3-x}Eu_xNb_5O_{15}$ is also negative for all x and T values but the absolute values increase near the MI phase boundary, as shown in Fig. 8(b), where $|R_{ac}|$ is plotted on a logarithm scale. Figure 8(c) shows the x dependence of the number of carriers per Nb, N, converted from the number of carriers per unit volume n, which was estimated from the absolute value of R_{ac} at 30 K by the relation

$$|R_{ac}| = \frac{1}{ne}. \tag{1}$$

As can be seen, N decreases from $\sim 10^{-1}$ at $x = 1$ to $\sim 10^{-3}$ at $x = 2.2$. Together with the T dependence of the resistivity ρ for $Ba_{3-x}Eu_xNb_5O_{15}$ shown in Fig. 3, it can be speculated that a metal-insulator transition occurs owing to the continuous decrease in the number of carriers with x.

Reflectivity spectra for the parent compound $Ba_2RNb_5O_{15}$. with R = La and Pr, and $Ba_{3-x}Eu_xNb_5O_{15}$, and the optical conductivity spectra obtained by the Kramers-Kronig transformation of those reflectivity spectra are shown in Figs. 9 ($Ba_2RNb_5O_{15}$) and 10 ($Ba_{3-x}Eu_xNb_5O_{15}$). First, for all the compounds, the reflectivity with the polarization along the *c* axis [$R_c(\omega)$] is higher than that along the *a* axis [$R_a(\omega)$] below 1 eV, and the position of the plasma edge $\hbar\omega_p$ [represented by triangles in Figs. 9(a) and 9(b)] is located at higher $\hbar\omega$ values for $R_c(\omega)$ than for $R_a(\omega)$. For the optical conductivity spectra $\sigma_c(\omega)$ and $\sigma_a(\omega)$ shown in Figs. 9(c) and 9(d), which are obtained by the Kramers-Kronig transformation of $R_c(\omega)$ and $R_a(\omega)$, the spectral weight for $\sigma_c(\omega)$ below 1 eV is larger than that for $\sigma_a(\omega)$ for all the compounds. This means that the compound is more conducting along the *c* axis even with the R substitution, consistent with the result obtained for resistivity.

With the substitution of Ba by trivalent La or Pr, $R_c(\omega)$ below 1 eV decreases but the position of the plasma edge $\hbar\omega_p$ barely changes [Fig. 9(a)]. The $\sigma_c(\omega)$ spectrum changes from a Drude-type spectrum [meaning that $\sigma_c(\omega)$ is maximum at $\hbar\omega = 0$ eV] for the parent compound to the spectrum with a peak at finite $\hbar\omega$ for the Pr-doped compounds [Fig. 9(c)]. On the other hand, the reflectivity of the parent compound and that of $Ba_{3-x}Eu_xNb_5O_{15}$ with $x = 1$ are barely different but with a further increase in x more than 1, the reflectivity below 1 eV decreases and $\hbar\omega_p$ shifts to lower energies [Fig. 10(a)]. As a result, the spectral weight of $\sigma_c(\omega)$ below 1.4 eV is heavily suppressed when $x > 1$ [Fig. 10(c)].

To estimate the Drude weight, the $\sigma_c(\omega)$ and $\sigma_a(\omega)$ spectra for these compounds were integrated up to 1.4 eV and are plotted as a function of x in Fig. 11. In the same figure, the Drude weight for $Ba_{3-x}Sr_xNb_5O_{15}$ [15] is also plotted as comparison. Note that the Drude weight is given by

$$D = \frac{\pi ne^2}{2m^*}, \tag{2}$$

where m^* is the effective mass of the carriers and n is the number of carriers per unit volume. First, the Drude weight for σ_c (closed symbols in Fig. 11) is approximately two times larger than that for σ_a (open symbols in Fig. 11) when x is less

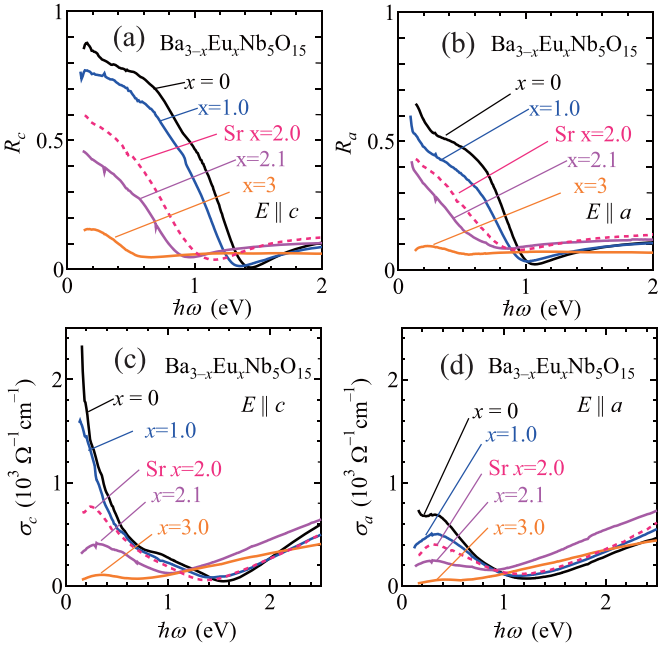

FIG. 10. (a), (b) Reflectivity and (c), (d) optical conductivity spectra with the polarization along the (a), (c) c and (b), (d) a axes for $Ba_{3-x}Eu_xNb_5O_{15}$. The dashed lines are the spectra for $Ba_{3-x}Sr_xNb_5O_{15}$ with $x = 2$ for comparison.

than 2. Furthermore, the Drude weight barely changes with the substitution of Ba by R up to $x = 1$ but it decreases when x becomes larger than 1 for $R =$ Eu. This result is qualitatively consistent with the metal-insulator transition observed in the resistivity of this series of compounds, although the Drude weight for $x = 2.1$ is not as small as suggested by the number of carriers estimated from the Hall coefficient shown in Fig. 8. Note also that the $\sigma_c(\omega)$ spectrum for $Ba_{3-x}Eu_xNb_5O_{15}$ with $x = 2.1$ is similar to that for $Ba_{3-x}Sr_xNb_5O_{15}$ with $x = 2$ [15] shown by dashed lines in Fig. 10. Furthermore, the x dependence of the Drude weight shown in Fig. 11 is similar to each other between $Ba_{3-x}Eu_xNb_5O_{15}$ and $Ba_{3-x}Sr_xNb_5O_{15}$. These results indicate that the characteristics of the metal-insulator transition are similar between these two series of compounds.

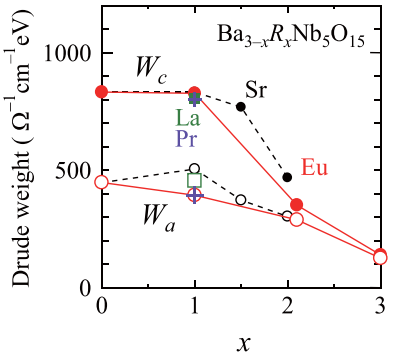

FIG. 11. Spectral weight of the optical conductivity up to 1.4 eV along the c (closed symbols) and a (open symbols) axes as a function of x for $Ba_{3-x}R_xNb_5O_{15}$ with $R =$ Eu (circles), La (a square), and Pr (a cross). Small circles are the data for $Ba_{3-x}Sr_xNb_5O_{15}$ for comparison.

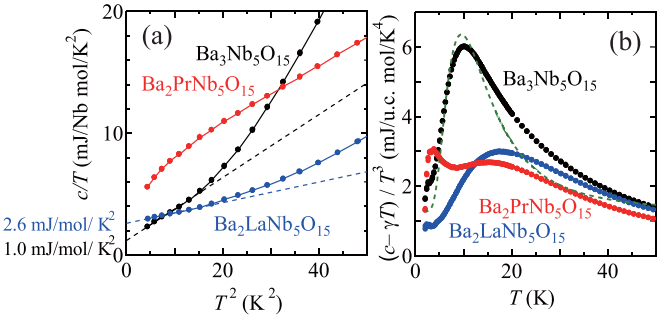

FIG. 12. (a) Specific heat c per molar Nb divided by temperature T as a function of T^2 for $Ba_3Nb_5O_{15}$ and $Ba_2RNb_5O_{15}$ with $R =$ La and Pr. (b) Specific heat c per molar unit cell ($Ba_6Nb_{10}O_{30}$) minus the linear term γT, which is divided by T^3, as a function of T for $Ba_3Nb_5O_{15}$ and $Ba_2RNb_5O_{15}$ with $R =$ La and Pr. The dashed line indicates the contribution of optical phonon modes with $\hbar\omega/k_B =$ 47 K.

To further study the electronic states near the Fermi level contributing to the transport properties, we measured the specific heat of $Ba_3Nb_5O_{15}$ and $Ba_2RNb_5O_{15}$ with $R =$ La and Pr. Figure 12(a) shows the specific heat c per molar Nb divided by T as a function of T^2. The electronic specific-heat coefficient γ, which appears as γT for c and corresponds to the y intercept of the graph, is given by

$$\gamma = \frac{\pi^2}{3} k_B^2 T g(\mathcal{E}_F) v, \tag{3}$$

where $g(\mathcal{E}_F)$ is the density of states at the Fermi energy and v is the molar volume. This means that γ is proportional to $m^* n^{1/3}$. It was fund that experimentally obtained γ increases from 1 mJ/Nb mol K^2 for $Ba_3Nb_5O_{15}$, which amounts to the density of states per Nb of 0.4 eV^{-1}, to 2.6 mJ/Nb mol K^2 for $Ba_2LaNb_5O_{15}$, which amounts to 1.1 eV^{-1}. This indicates that either the effective mass m^* or the number of carriers n (or both) increases with La doping.

On the other hand, the seemingly large c/T for $Ba_2PrNb_5O_{15}$ in Fig. 12 is likely due to the contribution of the magnetic moments of Pr. As shown in Fig. 7(b), the magnetic susceptibility for the Pr-doped compound does not diverge at the lowest T. This can be explained either by a strong antiferromagnetic interaction between the Pr moments or a spin-singlet ground state of the Pr^{3+} ions in this compound. In either case, the entropy of the Pr moments can contribute to the specific heat in the T range shown in Fig. 12(a) and to a small peak below 10 K in the data of $Ba_2PrNb_5O_{15}$ shown in Fig. 12(b). The analysis of the T dependence of the specific heat for this contribution is difficult and is not conducted in this paper.

In the graph of c/T vs T^2 [Fig. 12(a)], the contribution of phonon specific heat, which is proportional to T^3 as $c = \beta T^3$, is supposed to appear as the slope of a straight line. However, the curve for the parent compound clearly deviates from a straight line but increases in a superlinear manner, indicating that the specific heat whose T dependence is different from either γT or βT^3 exists at a low T. To see this more clearly, the contribution of the electronic specific heat γT is subtracted from c, and divided by T^3, and the result is plotted

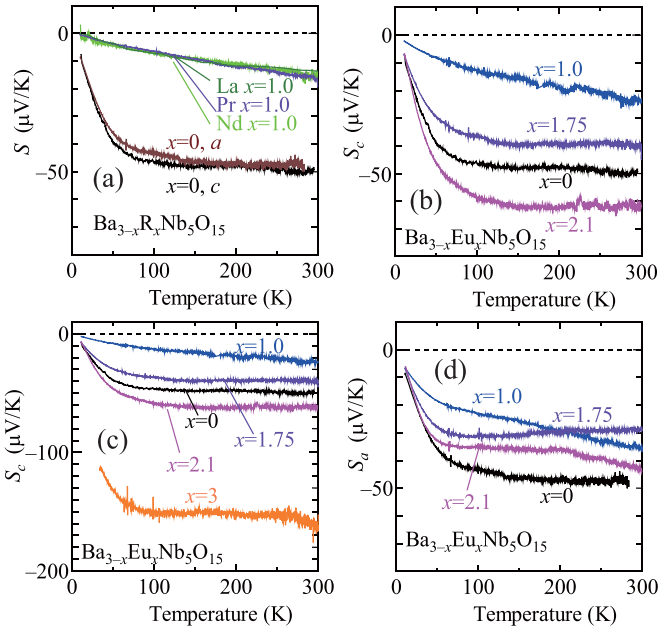

FIG. 13. (a) Temperature dependence of the Seebeck coefficient for $Ba_3Nb_5O_{15}$ along both the c axis [$S_c(T)$] and the a axis [$S_a(T)$] and for $Ba_2RNb_5O_{15}$ with R = La, Pr, and Nd along the c axis [$S_c(T)$]. (b), (c) Temperature dependence of the Seebeck coefficient along the c axis for $Ba_{3-x}Eu_xNb_5O_{15}$ with (b) $0 \leqslant x \leqslant 2.1$ and (c) $0 \leqslant x \leqslant 3.0$. (d) Temperature dependence of the Seebeck coefficient along the a axis for $Ba_{3-x}Eu_xNb_5O_{15}$ with $0 \leqslant x \leqslant 2.1$.

as a function of T in Fig. 12(b). If the specific heat is given by the sum of only the electronic contribution γT and the phonon contribution βT^3, this becomes a T-independent value of β. However, Fig. 12(b) clearly shows a large peak, particularly for the parent compound. We found that the specific heat of $Ba_3Nb_5O_{15}$ can be approximately fitted by the contribution of an Einstein mode plus a T^3 term and a T term, namely,

$$c = 3R\frac{(\hbar\omega_0)^2 \exp(\hbar\omega_0/k_BT)}{\{\exp(\hbar\omega_0/k_BT) - 1\}^2} + \beta T^3 + \gamma T, \qquad (4)$$

with a frequency of $\hbar\omega_0/k_B = 47$ K, $\beta = 1.3$ mJ/u.c. mol/K^4, and $\gamma = 1.0$ mJ/Nb mol/K^2, as shown by a dashed line in Fig. 12(b). By La or Pr doping, however, this peak is substantially suppressed. This suggests that these modes with $\hbar\omega/k_B = 47$ K are optical phonon modes associated with the motion of heavy Ba ions in $Ba_3Nb_5O_{15}$. A similar behavior of specific heat has been observed in materials with open structures [19].

We measured the thermopower of these compounds to clarify the change in charge dynamics with the substitution of R for Ba in the series of compounds. Figure 13(a) shows the T dependence of the Seebeck coefficient along the c axis $S_c(T)$ and along the a axis $S_a(T)$ for the parent compound, and $S_c(T)$ for $Ba_2RNb_5O_{15}$ with R = La, Pr, and Nd. $S(T)$ is negative for all the compounds over the entire T range. $S_c(T)$ and $S_a(T)$ for the parent compound are ~ -50 μV/K at 300 K, which is consistent with the value reported in Ref. [15]. $S_c(T)$ is nearly constant down to 50 K but below that temperature, its absolute value $|S_c(T)|$ sharply decreases toward 0 almost linearly with T. For $Ba_2RNb_5O_{15}$ with any R, $S(T)$ at 300 K

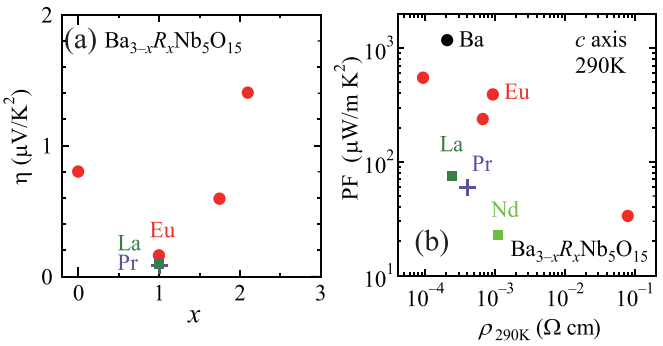

FIG. 14. (a) Coefficient of the T-linear term in the Seebeck coefficient along the c axis, η, for $Ba_{3-x}R_xNb_5O_{15}$ with R = Eu (circles), La (a square), and Pr (a cross). (b) Thermoelectric power factor S^2/ρ at 290 K as a function the resistivity at 290 K for $Ba_{3-x}R_xNb_5O_{15}$ with R = Eu, La, Pr, and Nd. Note that $x = 0$ is depicted as Ba.

is only ~ -15 μV/K and $|S_c(T)|$ decreases almost linearly with T from 300 K to the lowest T.

Figures 13(b) and 13(c) show $S_c(T)$ for $Ba_{3-x}Eu_xNb_5O_{15}$ with various x values. $|S_c(T)|$ at 300 K decreases to $\sim$15 μV/K and exhibits an almost T-linear behavior, similarly to the compounds with the substitution by trivalent R. With a further increase in x, however, $|S_c(T)|$ increases again and at $x = 2.1$, $|S_c(T)|$ exceeds that at $x = 0$. At $x = 3$ ($Eu_3Nb_5O_{15}$), $|S_c(T)|$ at 300 K amounts to 150 μK/V [Fig. 13(c)]. Note that the Seebeck coefficient of $Eu_3Nb_5O_{15}$ below 40 K cannot be measured because of the too large resistivity. As shown in Fig. 13(d), the Seebeck coefficient along the a axis [$S_a(T)$] behaves similarly to $S_c(T)$.

The Seebeck coefficient of metals, where $k_BR \ll \mathcal{E}_F$ holds, is generally given by

$$|S| = \frac{\pi^2}{2}\frac{k_B^2 T}{e\mathcal{E}_F}, \qquad (5)$$

where $\mathcal{E}_F$ is the Fermi energy. This means that $|S|$ is proportional to T at a low T ($|S| = \eta T$), and the coefficient η of the T-linear term is inversely proportional to $\mathcal{E}_F$. Note that if the condition $k_BR \ll \mathcal{E}_F$ is not satisfied, $|S(T)|$ tends to saturate with increased T, resulting in the nearly T-independent behavior for $x = 0$ above 50 K, for example. The coefficient η estimated from the experimentally obtained $S(T)$ at low T is plotted as a function of x in Fig. 14(a). As can be seen, η first decreases from $x = 0$ to 1, and then it increases with increasing x. The increase in η for $x > 1$ is consistent with the metal-insulator transition occurring at $x \sim 2.2$ with a continuous decrease in the number of carriers, which results in the decrease in $\mathcal{E}_F$. The decrease in η from $x = 0$ to 1 will be discussed in the next section.

The thermoelectric power factor S^2/ρ at 290 K is plotted as a function of the resistivity in Fig. 14. Although the Seebeck coefficient becomes larger with Eu doping for $Ba_{3-x}Eu_xNb_5O_{15}$, the power factor becomes smaller with Eu doping because of the increase in the resistivity. The thermoelectric power factor was found to be the largest for the parent compound, $Ba_3Nb_5O_{15}$.

IV. DISCUSSIONS

In this study, we measured six different physical quantities, namely, the resistivity ρ, the magnetic susceptibility χ, the Hall coefficient R_{ac}, the optical conductivity $\sigma(\omega)$, the specific heat c, and the Seebeck coefficient S. Among them, R_{ac}, the Drude weight D obtained using $\sigma(\omega)$, the electronic specific-heat coefficient γ obtained using c, and $S = \eta T$ are the quantities whose magnitudes are determined solely by the effective mass m^* and the number of carriers n. Namely, R_{ac}, D, γ, and η are given by Eqs. (1), (2), (3), and (5), respectively, and are related to m^* and n as $|R_{ac}| \propto n^{-1}$, $D \propto m^{*-1}n$, $\gamma \propto m^* n^{1/3}$, and $\eta \propto m^* n^{-2/3}$.

Let us discuss the dependence of these quantities on R based on these relations. First, with the R^{3+} substitution, the number of carriers n estimated from the Hall coefficient increases [Fig. 8(c)]. Nevertheless, the Drude weight, which is proportional to $m^{*-1}n$, barely changes (Fig. 11). This indicates that m^* increases with x for the R^{3+} substitution. This result is also consistent with the increase in the electronic specific-heat coefficient γ with La substitution [Fig. 12(a)]. According to a band calculation of $Ba_3Nb_5O_{15}$ [15], when the number of electrons per Nb is less than 0.1, there is a large dispersion along k_z for the bands crossing the Fermi level, resulting in planelike Fermi surfaces along the k_x-k_y plane. However, when the number of electrons is 0.2, the band dispersion around the Fermi level along k_z becomes smaller and one of the Fermi surfaces becomes cylindrical along the k_z direction. This indicates the increase in effective mass along the c axis with n, which is consistent with the present experimental results.

However, it does not seem compatible with the behavior of the coefficient of the T-linear term in the Seebeck coefficient η, which should be proportional to $m^* n^{-2/3}$ but substantially decreases by a factor of $\sim$10 with the substitution of R^{3+} [Fig. 14(a)].

With the Eu^{2+} substitution, η decreases from $x = 0$ to 1 more significantly compared with small changes in R_{ac} and D. With a further increase in x for $Ba_{3-x}Eu_xNb_5O_{15}$, near the metal-insulator phase boundary at $x \sim 2$, n decreases by two orders of magnitude as shown in Fig. 8(c). D also decreases with x (Fig. 11) but not as significantly as suggested by n estimated from $|R_{ac}|$. On the basis of the fact that the $\sigma(\omega)$ spectra are measured at room temperature and D is estimated as the spectral weight up to 1.4 eV, we speculate that part of the Drude spectrum at room temperature will separate and form a real Drude spectrum with much smaller spectral weight at low T. The increase in η with $x > 1$ is also consistent with the change in n if one considers the values of both n estimated from $|R_{ac}|$ and η at $x = 1$ as reference values for them at other x values but ignores the results at $x = 0$ [Fig. 14(a)]. This means that the behaviors of R_{ac}, D, and γ for $Ba_{3-x}Eu_xNb_5O_{15}$ and $Ba_2RNb_5O_{15}$ are consistent with each other, but the behavior of S is not consistent with that of other quantities near $x = 0$. It can be speculated that the coefficient of the T-linear term in S, η, for the parent compound is larger than that expected from the values of m^* and n, which results in the anomalous decrease in η with the substitution of R despite the absence of corresponding changes in m^* and n.

At present, we do not have a clear explanation for the anomaly in the Seebeck coefficient near $x = 0$ but we point out the experimental result that $d\rho_a/dT$ is negative whereas $d\rho_c/dT$ is positive below 100 K only for $x = 0$ [Fig. 5(a)]. This result can be explained by thermally excited carriers contributing to the electrical conduction perpendicular to the chain direction (Fig. 1). That is, for $x = 0$, even at temperatures below 100 K, thermally excited carriers contribute more to the conductivity along the a axis than the electrons near the Fermi level do. This means that metallic conduction exists only along the c axis at temperatures below 100 K in $Ba_3Nb_5O_{15}$. Such one dimensionality may be the origin of the anomaly in the Seebeck coefficient, i.e., larger values at $x = 0$, which disappears in the R-doped compounds because of the appearance of the three-dimensional conduction. Note that the increase in Seebeck coefficient in a two-dimensional structure has been observed in $SrTiO_3$ [20].

Note that a large negative magnetoresistance of $Ba_{3-x}Eu_xNb_5O_{15}$ occurs in the x and T ranges where $|R_{ac}|$ increases. This means that the large negative magnetoresistance is caused by the extremely small number of carriers near the metal-insulator phase boundary. This reminds us of the large negative magnetoresistance observed in EuO and Eu chalcogenides [21–23]. In these so-called magnetic semiconductors, the stoichiometric compounds are band insulators with magnetic moment on Eu but a small number of conduction carriers can be introduced by offstoichiometry or intentional doping, and they can be coupled with the magnetic moment of Eu, resulting in magnetic polarons and a large negative magnetoresistance. In $Ba_{3-x}Eu_xNb_5O_{15}$, although the origin of the small number of conduction carriers may be different from that in magnetic semiconductors, the existence of a small number of conduction carriers in the sea of a large number of magnetic moments of Eu is a common feature of magnetic semiconductors and $Ba_{3-x}Eu_xNb_5O_{15}$, and is likely related to the large negative magnetoresistance. Note that after the discovery of the large magnetoresistance of $Ba_{3-x}Eu_xNb_5O_{15}$ [16], a similar negative magnetoresistance has been reported for $EuNbO_{3-x}N_x$ [24].

Since the change in the optical conductivity spectra of $Ba_{3-x}Eu_xNb_5O_{15}$ with x is similar to that of $Ba_{3-x}Sr_xNb_5O_{15}$, as shown in Figs. 10 and 11, the origin of the metal-insulator transition may be disorder [15]. Namely, there are two sites for the Ba and Eu ions, A1 and A2 sites (Fig. 1), and since the ion at the A1 site is tightly connected to the surrounding oxygen ions, the Eu ions with a smaller ionic radius than Ba first occupy the A1 site up to $x = 1$ and, then, they start to occupy the A2 site when $x > 1$. Since the ion at the A2 site is only loosely bounded to the surrounding oxygen ions, a small Eu ion at the A2 site is likely located at several possible positions with local energy minima randomly, resulting in disorder in the crystal structure when $x > 1$. However, disorder alone may not be able to explain the reduction of the carriers near the metal-insulator phase boundary as observed in the Hall measurement, but it suggests the important role of the Coulomb interaction between the $4d$ electrons, which causes the so-called Coulomb gap in the density of states of the conduction electrons [25,26]. This scenario is roughly consistent with the change in the optical conductivity from a Drude-type spectrum to a spectrum with a peak at a finite $\hbar\omega$

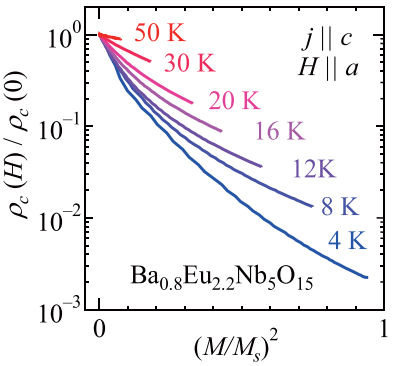

FIG. 15. Resistivity normalized to the value at $H = 0$ as a function of $(M/M_s)^2$ for $Ba_{3-x}Eu_xNb_5O_{15}$ with $x = 2.2$. M_s is a theoretical value of the saturation magnetization per mole for $x = 2.2$.

with increasing x. Note, however, that the T dependence of the Hall coefficient shown in Fig. 8(b) seems to suggest that the coupling between the Eu spins and the conduction electrons in the Nb 4d states is also responsible for the decrease in the number of conduction carriers.

The large magnetoresistance in $Ba_{3-x}Eu_xNb_5O_{15}$ near the metal-insulator phase boundary may be related to the physics of negative magnetoresistance in disordered systems [26–28]. However, the coupling between the itinerant electrons in the Nb 4d states and the localized spins at the Eu site must be considered in addition to disorder to explain the large negative magnetoresistance in this series of compounds. In Ref. [16], the resistivity divided by the value at $H = 0$ is plotted as a function of $(M/M_s)^2$ for $Ba_{3-x}Eu_xNb_5O_{15}$ with $x = 2.0$, where M is the magnetization experimentally obtained and M_s is the theoretical value of saturation magnetization. The data at different temperatures were found to approximately merge, indicating that negative magnetoresistance scales with M^2 for $x = 2.0$. The same plot has been performed for $x = 2.2$, as shown in Fig. 15, but the data at different temperatures do not merge for this composition close to the metal-insulator phase boundary. One possible origin of this deviation is the T dependence of carrier concentration n as suggested by the Hall coefficient R_{ac} in Fig. 8. Namely, the decrease in n results in the increase in the magnetoresistance and the deviation from the M^2 scaling.

V. SUMMARY

We grew single crystals of $Ba_{3-x}Eu_xNb_5O_{15}$ for $0 \leqslant x \leqslant 3$ and $Ba_2RNb_5O_{15}$ with R^{3+} = La, Ce, Pr, Nd, and Sm, and measured their various physical properties. $Ba_2RNb_5O_{15}$ is metallic irrespective of the species of R, whereas a metal-insulator transition occurs in $Ba_{3-x}Eu_xNb_5O_{15}$ at $x \sim 2.2$. Negative magnetoresistance observed in the Eu-substituted compounds increases near the metal-insulator phase boundary at $x \sim 2.2$. The sign of the Hall coefficient is negative for all the compounds, and the absolute value of the Hall coefficient decreases with R^{3+} substitution, consistent with the increase in the nominal number of electrons in Nb. The absolute values of the Hall coefficient for the Eu-substituted compounds increase by two orders of magnitude near the metal-insulator phase boundary, indicating a continuous decrease in the number of electrons upon the metal-insulator phase transition. The Drude weight of the optical conductivity spectrum along the c axis is larger than that along the a axis for all the compounds, indicating a higher electrical conduction along the c axis. The Drude weight along the c axis slightly decreases in the R^{3+}-substituted compounds, and substantially decreases for the Eu^{2+}-substituted compounds as they approach the metal-insulator phase boundary.

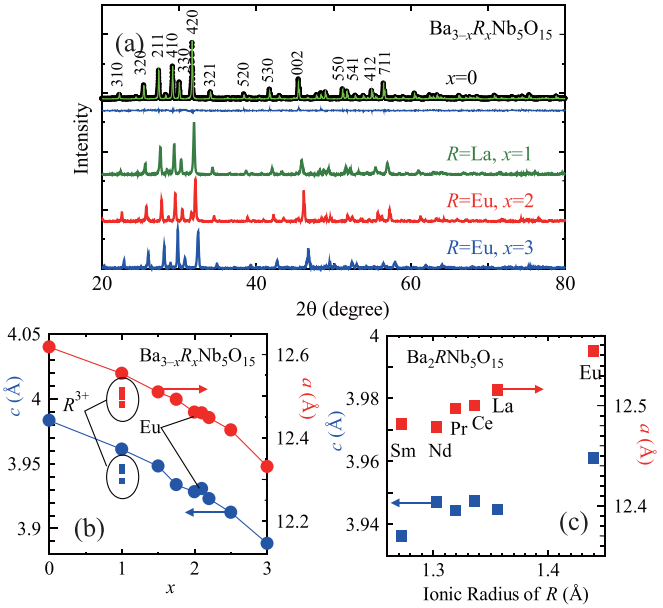

FIG. 16. (a) X-ray diffraction patterns of $Ba_3Nb_5O_{15}$, $Ba_{3-x}R_xNb_5O_{15}$ with R = La and $x = 1$, and with R = Eu and $x = 2$ and 3. For $Ba_3Nb_5O_{15}$, a Rietveld refinement pattern and the difference between the observed and calculated intensities are also plotted. (b) Lattice constants as a function of x for $Ba_{3-x}R_xNb_5O_{15}$. (c) Lattice constants of $Ba_2RNb_5O_{15}$ as a function of the ionic radius of R.

The electronic specific-heat coefficient increases with La^{3+} substitution. The Seebeck coefficient is negative for all the compounds, and for the parent compound, it is nearly constant at ~ -50 μV/K from 300 to 50 K, and then the absolute value decreases linearly with T below 50 K. With the R^{3+} or Eu substitution at $x = 1$, the absolute value of the Seebeck coefficient substantially decreases to $\sim$15 μV/K, but with a further increase in the Eu substitution, it increases again.

These experimental results can be explained by an increase in the number of carriers n and an increase in the effective mass m^* for the R^{3+} substitution, and a substantial decrease in n for the Eu^{3+} substitution near the metal-insulator

TABLE I. Valence of Nb obtained by thermogravimetric analysis (TGA).

Sample	Nominal valence of Nb	Valence of Nb by TGA	Number of d electrons per Nb
$Ba_3Nb_5O_{15}$	4.8	4.83	0.17
$Ba_2Eu_1Nb_5O_{15}$	4.8	4.81	0.19
$Ba_{1.9}Eu_{2.1}Nb_5O_{15}$	4.8	4.82	0.18
$Eu_3Nb_5O_{15}$	4.8	4.94	0.06
$Ba_2La_1Nb_5O_{15}$	4.6	4.63	0.37

TABLE II. Effective moment p and Weiss temperature θ obtained by the Curies-Weiss fitting of the susceptibility along the c axis. For the fitting, the data in the following ranges of T were used. (1) Ce: $50 < T < 300$ K; (2) Pr: $0 < T < 300$ K; (3) Nd: $80 < T < 300$ K; (4) Sm: $70 < T < 250$ K.

R	p	θ (K)	Theoretical p
Ce	2.44	44	2.54
Pr	4.23	78	3.58
Nd	3.85	52	3.63
Sm	1.23	550	0.84

phase boundary. Nevertheless, the behavior of the Seebeck coefficient near $x = 0$ cannot be explained by the changes in n or m^* but it suggests that the absolute value of the Seebeck coefficient at $x = 0$ is larger than that expected from the values of n and m^*. The possible origins of this discrepancy are the one-dimensional character of $x = 0$ and the change into the three-dimensional characters of the R-substituted compounds, as suggested by the sign of the temperature derivative of the resistivity. The present experimental results also indicate that negative magnetoresistance increases in the x and T ranges in which the number of carriers decreases substantially. This is similar to the behavior of the negative magnetoresistance of magnetic semiconductors, such as EuO and Eu chalcogenides, although the mechanism of the reduction in the number of carriers may be different.

ACKNOWLEDGMENTS

We thank T. Mizokawa and N. L. Saini for helpful discussions and H. Fukuyama for important suggestions. This work was supported by JSPS KAKENHI Grants No. 22H01172 and No. 22H04484. Magnetic susceptibility was measured using a shared research equipment (C1055) supported by the MEXT Project for promoting the public utilization of advanced research infrastructure (Grant No. JPMXS0440500023).

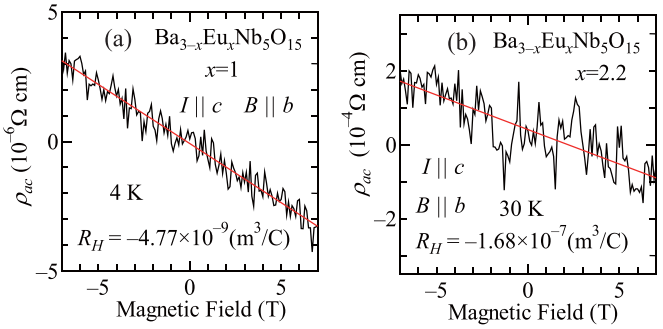

FIG. 17. Magnetic field dependence of the Hall resistivity for $Ba_{3-x}R_xNb_5O_{15}$ with $x = 1$ at 4 K and with $x = 2.2$ at 30 K.

APPENDIX

X-ray diffraction patterns of several samples and the lattice constants obtained from the x-ray diffraction are shown in Fig. 16.

The valence of Nb and the number of d electrons per Nb obtained by the thermogravimetric analysis of $Ba_{3-x}R_xNb_5O_{15}$ are shown in Table I. In the Curie-Weiss model, the magnetic susceptibility χ is given by the effective moment p and the Weiss temperature θ as

$$\chi = \frac{p^2\mu_B^2}{3(T+\theta)},$$

where μ_B is the Bohr magneton. The values of p and θ obtained by the fitting of the magnetic susceptibility along the c axis for $Ba_2RNb_5O_{15}$ are shown in Table II.

The magnetic field dependence of Hall resistivity is shown for two samples in Fig. 17. To remove the contribution of magnetoresistance, the difference between the Hall voltage at H and that at $-H$ was taken to calculate $\rho_{ac}(H)$. The result of the measurement from 7 to -7 T and that from -7 to 7 T are plotted in the positive and the negative sides of Fig. 17, respectively.

[1] M. Imada, A. Fujimori, and Y. Tokura, Metal-insulator transitions, Rev. Mod. Phys. **70**, 1039 (1998).
[2] N. Ali, M. Hill, S. Labroo, and J. Greedan, Magnetic and electrical properties of $R_2Mo_2O_7$ pyrochlore compounds, J. Solid State Chem. **83**, 178 (1989).
[3] T. Katsufuji, H. Y. Hwang, and S.-W. Cheong, Anomalous magnetotransport properties of $R_2Mo_2O_7$ near the magnetic phase boundary, Phys. Rev. Lett. **84**, 1998 (2000).
[4] N. Hanasaki, K. Watanabe, T. Ohtsuka, I. Kézsmárki, S. Iguchi, S. Miyasaka, and Y. Tokura, Nature of the transition between a ferromagnetic metal and a spin-glass insulator in pyrochlore molybdates, Phys. Rev. Lett. **99**, 086401 (2007).
[5] K. Matsuhira, M. Wakeshima, R. Nakanishi, T. Yamada, A. Nakamura, W. Kawano, S. Takagi, and Y. Hinatsu, Metal-insulator transition in pyrochlore iridates $Ln_2Ir_2O_7$ (Ln = Nd, Sm, and Eu), J. Phys. Soc. Jpn. **76**, 043706 (2007).
[6] K. Matsuhira, M. Wakeshima, Y. Hinatsu, and S. Takagi, Metal-insulator transitions in pyrochlore oxides $Ln_2Ir_2O_7$, J. Phys. Soc. Jpn. **80**, 094701 (2011).
[7] K. Ueda, J. Fujioka, and Y. Tokura, Variation of optical conductivity spectra in the course of bandwidth-controlled metal-insulator transitions in pyrochlore iridates, Phys. Rev. B **93**, 245120 (2016).
[8] S. Nakatsuji and Y. Maeno, Quasi-two-dimensional mott transition system $Ca_{2-x}Sr_xRuO_4$, Phys. Rev. Lett. **84**, 2666 (2000).
[9] V. I. Anisimov, I. A. Nekrasov, D. E. Kondakov, T. M. Rice, and M. Sigrist, Orbital-selective mott-insulator transition in $Ca_{2-x}Sr_xRuO_4$, Eur. Phys. J. B **25**, 191 (2002).
[10] B. Hessen, S. A. Sunshine, T. Siegrist, A. T. Fiory, and J. V. Waszczak, Structure and properties of reduced barium niobium oxide single crystals obtained from borate fluxes, Chem. Mater. **3**, 528 (1991).
[11] Y. K. Hwang and Y.-U. Kwon, Syntheses and electrical properties of tetragonal tungsten bronze type solid solution $Ba_{6-x}La_xNb_{10}O_{30+\delta}$ ($x = 0, 1, 2, 3$) and $Sr_6Nb_{10}O_{30}$, Mater. Res. Bull. **32**, 1495 (1997).
[12] T. Kolodiazhnyi, H. Sakurai, O. Vasylkiv, H. Borodianska, and Y. Mozharivskyj, Abnormal thermal conductivity in

tetragonal tungsten bronze $Ba_{6-x}Sr_xNb_{10}O_{30}$, Appl. Phys. Lett. **104**, 111903 (2014).

[13] T. Kolodiazhnyi, H. Sakurai, M. Isobe, Y. Matsushita, S. Forbes, Y. Mozharivskyj, T. J. S. Munsie, G. M. Luke, M. Gurak, and D. R. Clarke, Superconductivity and crystal structural origins of the metal-insulator transition in $Ba_{6-x}Sr_xNb_{10}O_{30}$ tetragonal tungsten bronzes, Phys. Rev. B **92**, 214508 (2015).

[14] T. Yasuda, Y. Kondo, T. Kajita, K. Murota, D. Ootsuki, Y. Takagi, A. Yasui, N. L. Saini, T. Katsufuji, and T. Mizokawa, Interplay between electronic correlation and atomic disorder in a low carrier density 4*d* transition-metal oxide, Phys. Rev. B **102**, 205133 (2020).

[15] Y. Kondoh, R. Takei, T. Okuda, K. Ueno, Y. Katayama, T. Saiki, W. Sekino, T. Kajita, and T. Katsufuji, Metal-insulator transition in $Ba_{3-x}Sr_xNb_5O_{15}$, Phys. Rev. B **104**, 125128 (2021).

[16] K. Iwamoto, W. Sekino, S. Ito, Y. Katayama, K. Ueno, and T. Katsufuji, Large negative magnetoresistance in $Ba_{3-x}Eu_xNb_5O_{15}$, J. Phys. Soc. Jpn. **91**, 033702 (2022).

[17] R. Nakamura, T. Miyoshino, Y. Kondoh, T. Kajita, T. Katsufuji, N. L. Saini, and T. Mizokawa, Electronic structure of $Ba_3Nb_5O_{15}$ and $Ba_2SrNb_5O_{15}$ studied by band calculation and photoemission spectroscopy, J. Phys. Soc. Jpn. **91**, 064711 (2022).

[18] K. Momma and F. Izumi, *VESTA 3* for three-dimensional visualization of crystal, volumetric and morphology data, J. Appl. Crystallogr. **44**, 1272 (2011).

[19] T. Takabatake, K. Suekuni, T. Nakayama, and E. Kaneshita, Phonon-glass electron-crystal thermoelectric clathrates: Experiments and theory, Rev. Mod. Phys. **86**, 669 (2014).

[20] H. Ohta, S. Kim, Y. Mune, T. Mizoguchi, K. Nomura, S. Ohta, T. Nomura, Y. Nakanishi, Y. Ikuhara, M. Hirano, H. Hosono, and K. Koumoto, Giant thermoelectric Seebeck coefficient of a two-dimensional electron gas in $SrTiO_3$, Nat. Mater. **6**, 129 (2007).

[21] A. Mauger and C. Godart, The magnetic, optical, and transport properties of representatives of a class of magnetic semiconductors: The europium chalcogenides, Phys. Rep. **141**, 51 (1986).

[22] M. R. Oliver, J. O. Dimmock, A. L. McWhorter, and T. B. Reed, Conductivity studies in europium oxide, Phys. Rev. B **5**, 1078 (1972).

[23] Y. Shapira, S. Foner, N. F. Oliveira, and T. B. Reed, EuTe. II. Resistivity and Hall effect, Phys. Rev. B **5**, 2647 (1972).

[24] T. Maruyama, Y. Hirose, T. Katayama, Y. Sugisawa, D. Sekiba, T. Hasegawa, and A. Chikamatsu, Negative magnetoresistance in different nitrogen content $EuNbO_{3-x}N_x$ single-crystalline thin films, J. Mater. Chem. C **10**, 14661 (2022).

[25] A. L. Efros and B. I. Shklovskii, Coulomb gap and low temperature conductivity of disordered systems, J. Phys. C: Solid State Phys. **8**, L49 (1975).

[26] P. A. Lee and T. V. Ramakrishnan, Disordered electronic systems, Rev. Mod. Phys. **57**, 287 (1985).

[27] P. A. Lee and T. V. Ramakrishnan, Magnetoresistance of weakly disordered electrons, Phys. Rev. B **26**, 4009 (1982).

[28] N. Kobayashi and Y. Muto, Anomalously large negative magnetoresistance of 1*T*-TaS_2 at ultra low temperatures, Solid State Commun. **30**, 337 (1979).